

Article

Improving Optical Performance of Ultraviolet Light-Emitting Diodes by Incorporating Boron Nitride Nanoparticles

Caiman Yan ¹, Qiliang Zhao ¹, Jiasheng Li ¹, Xinrui Ding ¹, Yong Tang ¹ and Zongtao Li ^{1,2,*} 

¹ Key Laboratory of Surface Functional Structure Manufacturing of Guangdong High Education Institutes, South China University of Technology, Guangzhou 510641, China

² Foshan Nationstar Optoelectronics Company Ltd., Foshan 528000, China

* Correspondence: meztli@scut.edu.cn; Tel.: +86-13824460886

Received: 4 June 2019; Accepted: 23 July 2019; Published: 26 July 2019



Abstract: Ultraviolet light-emitting diodes (UVLED) are a new type of device in the LED development; however, the radiant efficacy of UVLEDs is still too low to satisfy the requirements of applications. In this study, boron nitride nanoparticles (BN NPs) are incorporated into the UVLED's silicone encapsulation to improve the optical output power. This BN NPs-based package shows an increase in optical flux of 8.1% compared with silicone-only encapsulation when the BN NP concentration is optimized at 0.025 wt%. By analyzing the BN NP film, adding the BN NPs into silicone leads to a decrease in transmittance but an increase in haze. Haze and transmittance has an excellent negative correlation with increasing BN concentration under 365 nm. The moderate BN NP concentration maximizes the scattering performance from haze while maintaining high transmittance. Therefore, this enhanced light output is attributed to scattering that reduces optical losses from total internal reflection at the silicone–air interface. By using the new BN-based structure in green and red quantum dot devices, an increase radiant flux of the device is observed, 9.9% for green LED and 11.4% for red LED. This indicates that BN NPs have potential prospects in the application of UV LEDs used as excitation sources for quantum dots.

Keywords: BN nanoparticles; optical performance; quantum dots; ultraviolet light-emitting diode

1. Introduction

Light-emitting diodes (LEDs) have shown a surprising rate of development as a fundamental device for solid-state illumination and display [1–3]. Besides application in the visible spectrum, the LED has now extended into the ultraviolet (UVLED) [4,5]. By inheriting the advantages of LED such as small size, low cost, long life, and ecological environment protection, the UVLED is considered as one of the best choices to replace the traditional gas ultraviolet light source by eliminating a source of mercury pollution [6–8]. The UVLED exhibits outstanding prospects for application in ultraviolet illumination, displays, ultraviolet curing, anti-counterfeiting detection, and sterilization [9]. UV light can be divided into four levels according to its emission wavelength: UVA (320–400 nm), UVB (280–320 nm), UVC (200–280 nm), and UVD (100–200 nm) [10]. The UVA LED is likely to be the first to achieve commercialization.

However, UVLED with the short emission wavelength suffers a lower external quantum efficiency (EQE) than the blue LED [11,12]. This situation is worse in the deeper UV, such as with UVC or UVD LEDs [13]. Thus, the UVLED still has some challenges to meeting the harsh market requirements. The low EQE of UVLEDs mainly results from two factors: (1) In order to attain ultraviolet emission, the addition of Al in the epitaxial growth is inevitable. However, this high aluminum mole fractions

introduces a new challenge to the epitaxy process [14,15]. The huge difference in the lattice and thermal coefficient between AlGaIn layer and sapphire substrate results in high density of crystal defects like threading dislocations. These defects would serve as the non-radiative recombination centers. Compared with blue LED, the UVLED is more sensitive to non-radiative recombination centers because of the lack of indium-based localized states in multiple quantum well active regions. As the crystal quality is inferior to that of the blue LED chip, the internal quantum efficiency (IQE) is likewise greatly reduced. (2) In the package stage to protect the LED chip and meet the application requirement, the traditional blue LED chip package process is not completely suitable for the ultraviolet chip. For example, the all-inorganic package is more suitable for UVLEDs. Total internal reflection of some UV light greatly reduces the light emission [16,17], a condition that needs to be improved urgently. In addition, the energy that is not converted into light in a low-efficiency UVLED generates heat, which, if excessive, has a negative effect on the optical stability [18,19]. Reducing the thermal resistance of the device can improve the heat dissipation of the UVLED.

To lower the total reflection effect and improve the luminous efficiency, introducing nanoparticles (NPs) into the silicone encapsulation has proven to be simple and effective in blue LEDs. In previous research, we studied the role of introducing ZnO NPs into the silicone encapsulation of a quantum dot blue-LED application and found that the luminous flux was increased by 3.37% by adding a small amount of the ZnO NPs [20]. TiO₂ NPs added to a blue LED produce a similar result, with the luminous intensity increased by 31% at a concentration of 0.05 wt% [21]; this is consistent with the reports by Su, Wang, and Zheng [22–24]. However, these two solutions do not have the same benefits for UVLEDs. Due to the relatively small band gap, 3.1 eV for ZnO and 3.2 eV for TiO₂, both of them become light-absorbing in the ultraviolet, counteracting any scattering advantage. Therefore, a search for a non-UV absorbing nanoparticle for UVLEDs takes on great significance.

Quantum dots (QDs), taking advantages of their narrow spectral half width, high absorption coefficient, wide excitation spectrum, high quantum yield, and wide color range, have been a new area in LED research recently [25–27]. Their excellent properties make them a strong candidate for the next generation of semiconductor luminescent materials. Since QDs absorb UV light more strongly than visible light, UV LEDs may be a valuable excitation source for quantum dots in devices such as plant lighting, specialty lighting, and displays [28]. However, as the optical efficacy of UV LEDs is not high enough, the advantages of this strategy have not been realized. A reliable method to improve the performance of the entire quantum dot device is by increasing the optical intensity of the ultraviolet LED. Zhang et al. [29] mixed Al₂O₃ and SiO₂ particles in a traditional polymer lead frame. They found that its reflectivity at 365 nm could be increased to 54.4%, while having good thermal stability. Bas et al. [30] developed a special oligosiloxane material with less degradation in UV lighting for UVLED device packaging, which has a transmittance comparable to that of polydimethylsiloxane (PDMS) in the ultraviolet (>80%). Improving the UV reflectivity and reducing absorption of scattering nanoparticles are important directions for research on UV LED devices.

In this study, boron nitride nanoparticles (BN NPs) were selected from five nanomaterials; the candidates also included AlN, TiO₂, ZnO, and ZrO₂ NPs. A new packaging structure was proposed that incorporates 0.025 wt% BN NPs in the silicone encapsulation and experimental results showed that this structure enhances the light output power by 8.1%. Further, the underlying mechanism by which the BN NPs affect the optical properties of the LED was explored. It is also found that the BN NPs have advantages in reducing thermal resistance. The UVLED with 0.025 wt% BN NPs is then used to excite the quantum dots, and the optical properties of both green and red quantum dots are also improved.

2. Methods

2.1. Characterization

The nanoparticle materials including AlN, BN, TiO₂, ZnO, and ZrO₂ NPs were purchased from Shanghai Xiangtian Nano Materials Co., Ltd. and are of high purity grade. The PDMS silicone was bought from Dow Corning Corporation. The green and red quantum dots were acquired from Beijing Beida Jubang Science & Technology Co., Ltd.

The reflectance and absorbance of different NPs were tested directly by using an ultraviolet-visible spectrophotometer with an integrating sphere accessory (TU-1901, Persee, Beijing, China). The phase purity and structure of the BN NPs were measured using an X-ray diffractometer (D8-Advance, Bruker, Karlsruhe, Germany) with a Cu-K α radiation source ($\lambda = 0.15418$ nm) over the scanning angle range from 5 to 80°. The SEM image was captured by a scanning electronic microscope (SEM, Merlin, Zeiss, Oberkochen, Germany). The transmittance of the BN film was tested by a UV-vis spectrometer with an integrating sphere accessory (TU-1901, Persee, Beijing, China). As for haze, firstly, the diffusion and transmittance of the BN film were directly measured by a UV-vis spectrometer. Then the haze of the BN film was obtained by calculating the ratio of the diffusion to the transmission.

The photoluminescence (PL) spectrum and the absorption spectrum of the quantum dots film were collected by using a fluorescence spectrophotometer (RF-6000, Shimadzu, Japan) and a UV-vis spectrometer (TU-1901, Persee, Beijing, China). The electroluminescence (EL) spectra and optical parameters of the UVLED and QD-converted LED devices were measured by a calibrated integrating sphere system with a spectrometer (USB2000+, Ocean Optics, Largo, FL, USA) and a power supply (Keithley 2425, Keithley Instruments & Products, Cleveland, OH, USA). The thermal resistance of UVLEDs was tested by a semiconductor thermal transient tester (T3Ster, Simucad, Shanghai, China) under 400 mA at room temperature (25 °C). The summary of the equipment is shown in Table 1.

Table 1. The characteristics of equipment.

Equipment	Description
X-ray diffractometer	D8-Advance, Bruker, Karlsruhe, Germany
Scanning electronic microscope	Merlin, Zeiss, Germany
Fluorescence spectrophotometer	RF-6000, Shimadzu, Japan
Ultraviolet-visible spectrophotometer	TU-1901, Persee, China
Semiconductor thermal transient tester	T3ser, Simucad, China
Spectrometer	USB2000+, Ocean Optics, America
Power supply	Keithley 2425, America

2.2. Selection of Nanoparticles for the UVLED

To investigate the properties of different NPs under ultraviolet wavelengths, powders of different NPs were compressed at high pressure into a cake shape. By using the standard BaSO₄ sample to calibrate the baseline, the spectral reflectance and absorbance were tested. In Figure 1a, all the nanomaterials showed a high reflectivity (above 77%) from 450 to 780 nm. Specifically, the reflectance of AlN, BN, TiO₂, ZnO, and ZrO₂ NPs at 450 nm blue light are 77.8%, 95.5%, 90.2%, 94.2%, and 95.4% respectively, indicating that these nanomaterials had similar blue-light blocking performance. However, this situation completely changed on entering the ultraviolet range: BN nanoparticles continued to exhibit very high reflectance in the UVA (320–400 nm). The reflectance of ZrO₂ and AlN NPs in the ultraviolet decreased slightly, while the reflectance of TiO₂ and ZnO NPs declines dropped rapidly in the UVA. Sorted by reflectance (high to low), the order was BN > ZrO₂ > AlN > TiO₂ > ZnO for the typical 365 nm UVA wavelength. Specifically, BN, ZrO₂ and AlN nanoparticle still reflected 98.8%, 88.9%, and 73.5%, respectively, for UV light, while TiO₂ and ZnO NPs only showed 19.0% and 1.1% reflectivity at 365 nm. Similar behavior was shown in the absorbance in Figure 1b. The absorbance of these five kinds of nanoparticles was relatively low in the visible light region. However,

the absorbance of TiO₂ and ZnO NPs grew exponentially in the UVA region; with ZrO₂, the absorbance rose gradually, while for BN and AlN it remained relatively constant. At the typical UV wavelength of 365 nm, the absorption of the five particles (ordered from high to low) was just the opposite of the reflectance: BN < ZrO₂ < AlN < TiO₂ < ZnO. The underlying reason for this different behavior was the different band gaps: ZnO = 3.1 eV, TiO₂ = 3.2 eV, AlN = 6.2 eV, ZrO₂ = 4.3 eV, and BN = 5.2 eV. AlN NPs could not achieve an ideal reflectance here because the harsh preparation process of AlN NPs easily contained impurities and the AlN property was sensitive to impurities [31,32]. Thus, UVA photon energy such as 3.4 eV (365 nm) did not exceed the band gap for BN, AlN, or ZrO₂ but was high enough for TiO₂ and ZnO, resulting in the distinct UVA absorbance. Therefore, the TiO₂ and ZnO NPs were not suitable for a UVLED because the strong UV absorption lowered the light efficiency. Among the others, BN showed the highest reflectance and stable performance in the UVA region. In addition, BN NPs had a high refractive index ($n = \sim 1.7$), excellent thermal conductivity ($\sim 25.1 \text{ W m}^{-1} \text{ K}^{-1}$), and good chemical stability under UV radiation [33]. The BN NPs were accordingly selected for further study for UVLEDs.

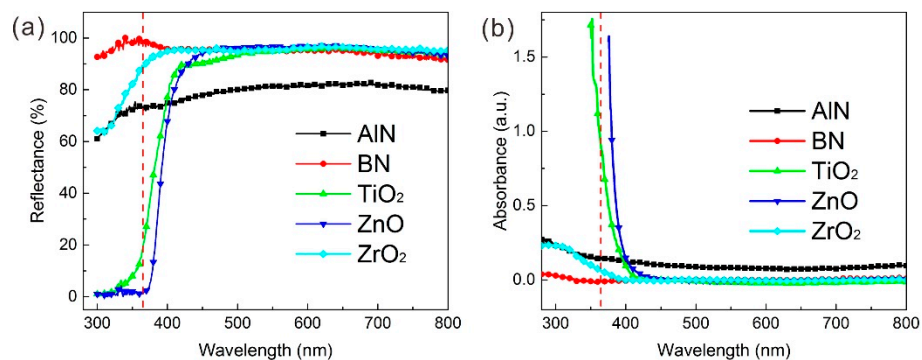


Figure 1. (a) The reflectance and (b) absorbance of AlN, BN, TiO₂, ZnO, and ZrO₂ nanoparticles (NPs); the dotted red line indicates 365 nm.

2.3. XRD Characteristic of BN Nanoparticles

The XRD characteristic of BN NPs is shown in Figure 2. All the diffraction peaks of the sample corresponded to the standard cards JCPDS: 34-0421, and the diffraction angles $2\theta = 26.7^\circ$, 41.7° , 43.8° , 50.1° , 55.1° , and 75.9° corresponded to the (002), (100), (101), (102), (004), and (110) crystal planes of BN NPs, respectively, showing that the NPs used in the experiment were hexagonal boron nitride. The XRD trace showed that the half width of each peak was extremely narrow, indicating that the BN NPs had high crystallinity and almost no impurities. The BN powders displayed an apparent white color under sunlight, an indirect confirmation of the excellent reflection characteristics of BN for visible light.

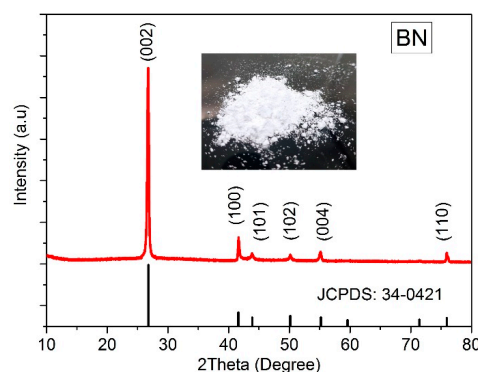


Figure 2. The XRD characteristic of the BN NPs.

2.4. SEM Image of BN Nanoparticles

From the scanning electronic microscopy (SEM) image shown in Figure 3, the BN material used in this study was on the nano-scale. The size of these BN NPs was about 400 nm and the structure tended toward sheet-like.

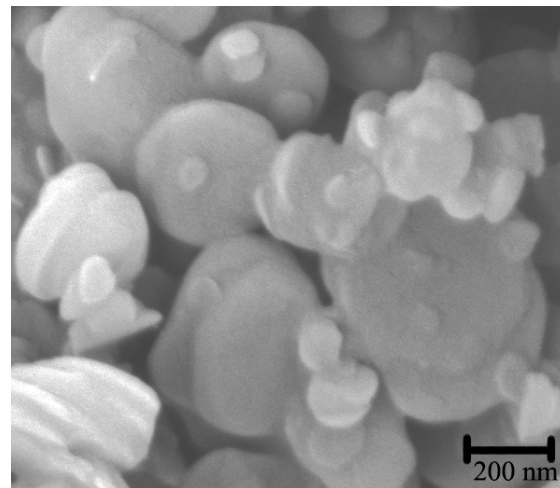


Figure 3. SEM image of the BN NPs.

2.5. Preparation of a UVLED Based on BN Nanoparticles

To fabricate the BN-based UVLED, a 365 nm LED chip (45 mil × 45 mil) was chosen as shown in Figure 4. After the UVLED was fixed onto the aluminum substrate, which served as the circuit board and heat sink, the gold wires were bonded by ultrasonic welding to complete the unit. At the same time, the polydimethylsiloxane (PDMS) silicone mixed with various concentrations of BN NPs was prepared. After vacuum defoaming, the PDMS–BN NP mixture was injected into the cavity of the UVLED. The entire device was then heated at 100 °C for 1 h to complete the packaging process. As a result, the BN-based UVLEDs, containing a weight ratio of 0.01, 0.025, 0.05, 0.1, and 0.2 wt% BN NPs in addition to a 0 wt% reference sample, were the experimental samples prepared for the study.

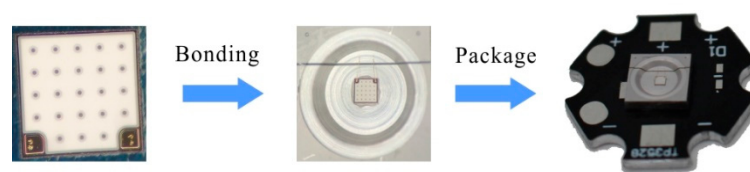


Figure 4. Packaging process of UV-light-emitting diodes (LEDs).

2.6. Preparation of BN Nanoparticle-Based Film and Quantum Dot Film

To investigate the mechanism of adding BN NPs into the package, different concentrations of BN films were prepared. Specifically, the PDMS mixed with the BN NPs was injected into a mold cavity designed to fabricate film whose thickness was set at 500 μm by a gasket. After annealing the die cavities for 1 h at 100 °C, the finished planar films could be prepared.

To prepare quantum dots (QDs) films for UV LEDs, green and red quantum dots were first selected, which had CdSe/ZnS and CdSe/ZnS/ZnS compositions, respectively. After dispersing in a small amount of n-hexane, the QDs were mixed with the PDMS. The PDMS used for the QD film was consistent with the silicone used for the UVLED package, eliminating any difference in refractive index. Then the film preparation was carried out using a designed mold. After 1 h of heating at 100 degrees, it could be released to obtain QD films.

3. Results and Discussion

The radiant flux and the electroluminescence (EL) spectra of different BN-based UVLEDs are shown in Figure 5. In Figure 5a, the radiant flux of all samples increased almost linearly with current, indicating that the performance of the UV chip was stable. With the increase of BN NPs, it could be seen that the radiant flux first rose, reached a maximum at 0.025 wt% BN concentration, and then dropped. The radiant flux versus BN concentration under different currents is given in Figure 5b. Apparently, the 0.025 wt% BN UVLED produced the highest radiant flux, among these samples. Specifically, at a current of 400 mA, the radiant flux of 0, 0.01, 0.025, 0.05, 0.1, and 0.2 wt% BN-based UVLEDs were 532.9, 576.8, 580.3, 566.9, 548.3, and 527.4 mW, respectively. Thus, the packaged UV-LED with a 0.025 wt% BN NPs increased the radiant flux by 8.8% compared with the reference. After testing 10 optimized BN-based LED devices, the average radiant flux increase at 400 mA was around 8.1%. The EL spectra for UVLEDs of different BN concentrations at 300 and 400 mA are shown in Figure 5c,d. The emission of the UV LED was at 369 nm with a half width of about 12 nm. It can be seen that the UVLED with 0.025 wt% BN NPs had the highest emission for both 300 and 400 mA current. Thus, from this experimental result, with 0.025 wt% BN NPs adding into silicone package for the UVA LED, the radiant flux was enhanced.

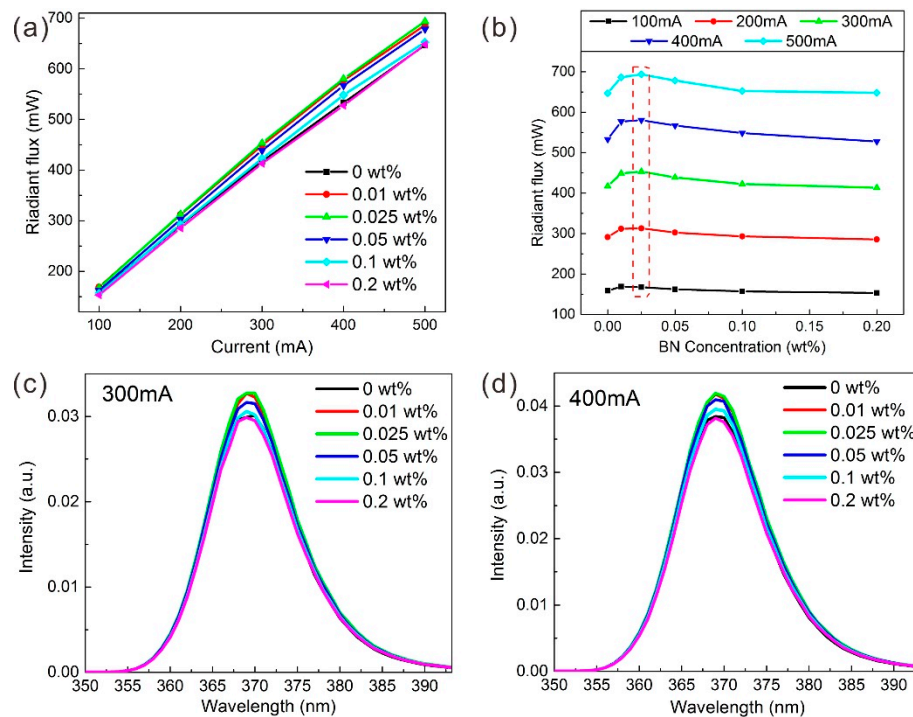


Figure 5. (a) The radiant flux of the UVLED versus current, for different BN concentrations; (b) the radiant flux versus BN concentration, for different currents. (c) The electroluminescence (EL) spectrum of the UVLED at 300 mA for different BN concentrations; (d) EL spectrum at 400 mA.

To investigate the process of adding BN NPs into the package, films with different concentrations of BN NPs were prepared. In Figure 6e, it is apparent that the transmittance of film is gradually reduced with increasing BN concentration. The data shows that at 365 nm, the transmittance of BN-based films with different concentrations was 94.0% (0 wt%), 93.3% (0.01 wt%), 91.6% (0.025 wt%), 88.4% (0.05 wt%), 77.6% (0.1 wt%), and 69.9% (0.2 wt%). The decrease in transmittance was the result of backscattering by the UV-resistant BN NPs. To evaluate the scattering, the concept of haze was introduced: Haze is defined as the ratio of intensities of the diffused light to the light passing through the BN film, expressed as a percentage. To obtain haze, firstly, the diffusion and transmittance of the BN film were directly measured by a UV-vis spectrometer. Then the haze could be calculated. Figure 6b

shows the haze versus wavelength for different BN concentrations in films. Without the NPs, the haze of the film was close to 0% from ultraviolet to visible; however with added BN NPs in the film, the haze through the whole wavelength range was enhanced gradually with concentration. Specially, the haze of various concentration BN-based films were 0.4% (0 wt%), 9.5% (0.01 wt%), 14.2% (0.025 wt%), 25.5% (0.05 wt%), 62.4% (0.1 wt%), and 84.8% (0.2 wt%) at 365 nm, so BN NPs could greatly increase the haze, with the haze reaching 84.8% at 0.2 wt%. This indicates the BN NPs had strong scattering properties. At higher BN concentrations such as 0.2 wt%, the UV scattering was stronger than the visible, supporting the experimental observation of transmission.

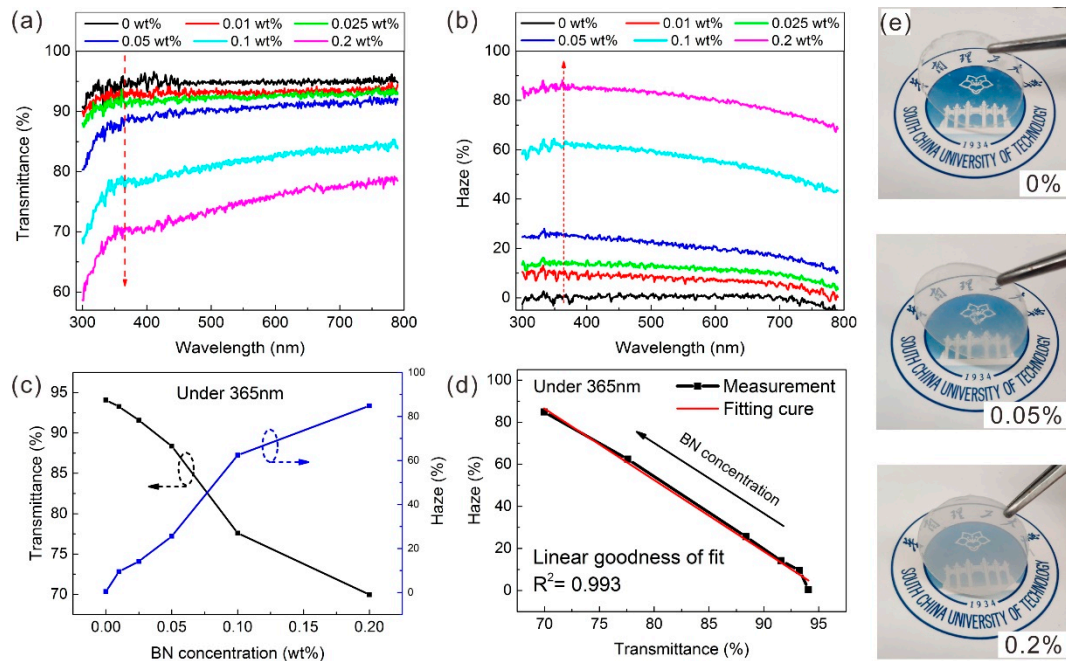


Figure 6. (a) The transmittance and (b) haze versus wavelength for different BN NP concentrations in a film. The red dotted line indicates 365 nm. (c) Transmittance and haze (experimental) versus BN concentration for wavelengths under 365 nm; (d) relationship between measured haze and transmittance; (e) photographs of BN films.

The dependence of measured transmittance and haze on BN concentration for wavelengths under 365 nm is shown in Figure 6c. It is easy to assume that the haze increases and the transmittance decreases gradually as the BN concentration increases. However, when plotting the transmittance versus the haze, with BN concentration as a parameter (Figure 6d), the haze had a very strong negative correlation with transmittance. Using a linear fitting function, the goodness of fit (R^2) was 0.993. The relationship between haze (H) and transmittance (T) of the BN NPs was described by the formula:

$$H = -3.3915 \times T + 323.83 \quad (1)$$

From the UVLED device test above, the radiant flux reached its peak at 0.025 wt% BN concentration. At this concentration, although the transmittance was lower than that of the reference film with 0 wt% BN NPs, the haze was much higher, showing that haze played a major positive role in improving the light output. From 0 to 0.025 wt%, radiant flux was increasing, but for a BN concentration over 0.025 wt%, the negative effect of the decrease in transmittance prevailed, which decreased the light output gradually.

With the addition of a small amount of BN NPs, the fundamental reason for the increase in the radiant flux of the UVLED was the reduction of total reflection. The propagation of light in different transmission media follows Snell's law. Due to the difference in refractive index between PDMS and

air, when the incidence angle of the ultraviolet was greater than the critical angle, total reflection occurs and the light was reflected back (Figure 7a). The critical angle was calculated using the total reflection formula:

$$\alpha = \arcsin(n_2/n_1), \quad (2)$$

where n_1 and n_2 represent the refractive index of air ($n_2 = 1$) and PDMS ($n_1 = 1.4$), respectively. The critical angle α of the film considered here is 45.5° . After adding the BN NPs, by taking advantage of the excellent UV light reflectance and scattering characteristic as discussed above, the BN NPs played an important role in the following two aspects illustrated by the deflected paths in Figure 7b. In one case, when UV light with an original incident angle greater than α propagates, a BN nanoparticle scatters the light and the final incident angle may be less than the critical angle, resulting in light exiting the LED. In the other case, UV light reflected by total reflection at the interface hits the BN nanoparticle and then may be scattered back; if it avoids total reflection, it will exit into the air. The degree of scattering promotes these light emission probabilities. Both these two processes reduce the extent of loss resulting from total reflection in the original UVLED. However, if the concentration of BN NPs is excessive, the decrease in light transmittance will dominate, and the probability of UV light arriving at the interface is reduced. Light that could not emit outside would be absorbed by the substrate and become heat, leading to a lowered emission.

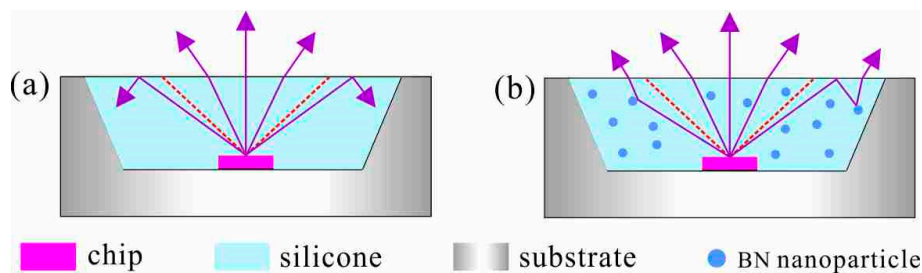


Figure 7. Schematic diagram of the UVLED (a) without BN or (b) with BN NPs. Dotted red lines indicate the incidence angle for total reflection.

To determine the thermal performance after adding BN NPs to the device, because the UVLED with 0.025 wt% BN NPs had the maximum light output, the comparison of radiant flux and thermal resistance between UVLED with 0 wt% and 0.025 wt% BN NPs groups under 400 mA was carried out in room temperature condition, as shown in Figure 8. The detail of thermal resistant could be found in our previous report [34]. The thermal resistance here refers to the thermal resistance from the LED chip to the lead frame of the UVLED device, including the LED chip, die attach layer and lead frame. Compared to the UVLED without BN NPs, 0.025 wt% BN-based UVLED not only had an advantage in radiant flux, but also had a lower thermal resistance. The thermal resistance of 0 wt% and 0.025 wt% BN-based UVLED was 4.66 and $3.68 \text{ K}\cdot\text{W}^{-1}$, respectively. The reduction in thermal resistance was mainly due to the improvement of UVLED light output. For LED, input electrical energy is mainly converted into light energy and heat energy. At moderate BN concentrations, the radiant flux of the UVLED was increased, so the thermal energy was reduced, resulting in a decreased thermal resistance. Moreover, lower thermal resistance of the device had a positive effect on the overall life of the UVLED.

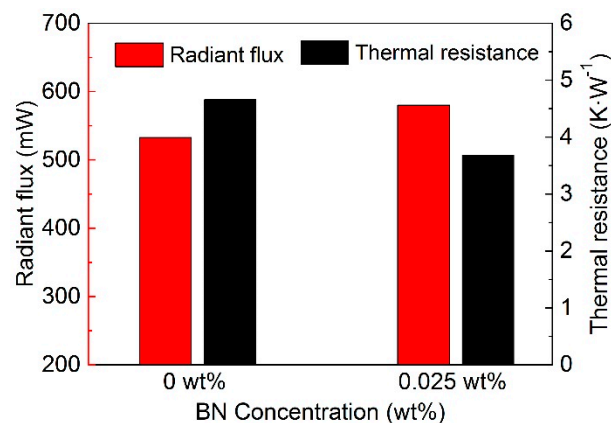


Figure 8. Comparison of radiant flux and thermal resistance between UVLED with 0 wt% and 0.025 wt% BN NPs groups under 400 mA. Radiant flux is indicated by red bars, thermal resistance by black bars.

Further, we studied the optical performance by incorporating BN NPs into the structure of a UVLED used to remotely excite quantum dot films. The absorbance and photoluminescence (PL) spectra of green and red QD films are shown in Figure 9. The emission peaks of green and red QD films were at 526 and 634 nm while the absorbance peaks were located at 516 and 606 nm, respectively. For both, the PL peak was at a longer wavelength than the absorbance peak. These results were from the Stokes effect and for the red quantum dots, with a larger particle size, the effect was more pronounced. The half widths of the green and red QD emission peaks were 27 and 30 nm, respectively, which were quite narrow compared to common fluorescent materials such as yttrium aluminum garnet (YAG) phosphors [35,36]. Both QDs had a higher absorption coefficient in the UVA region than in the visible.

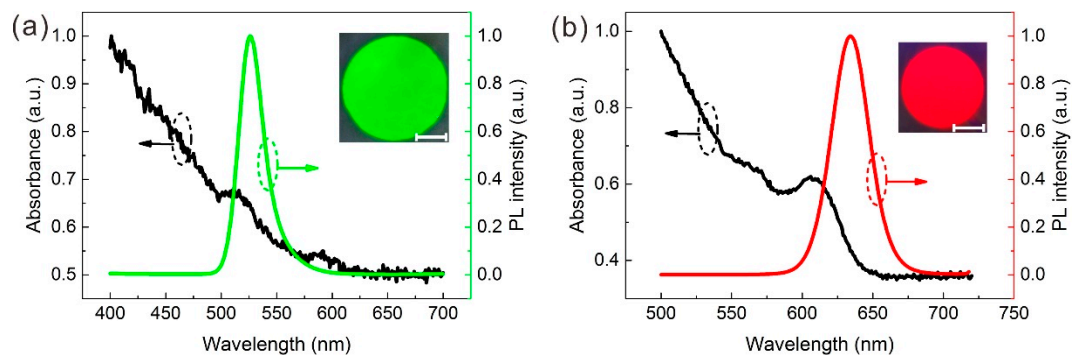


Figure 9. The absorbance and photoluminescence (PL) spectra of (a) green and (b) red quantum dot films. Inset are the physical pictures of films excited by 365 nm, white scale bar representing 2 mm.

For the application as an excitation source for the green QD film, Figure 10c shows that the UVLED with 0.025 wt% BN NPs produced a radiant flux that was higher than without the BN NPs. For a current of 500 mA, the radiant fluxes of the green LED devices without and with the BN NPs were 200.4 and 220.4 mW, respectively, an increase of 9.9%. The EL spectra of these two different green LED devices at 500 mA are shown in Figure 10d. The purple and green peaks from the UV LED chip and the green quantum dot film were located at 367 and 525 nm. The half width of the green peak was about 25 nm, which maintains the advantage of QDs. With the addition of 0.025 wt% BN NPs to the LED encapsulation, the ultraviolet peak intensity was decreased while the green peak was increased. With the BN NPs, more UV light from the chip was emitted into the QD film, which was converted to green light, resulting in a higher green peak and a lower purple peak. Therefore, the overall radiant flux of the device was increased.

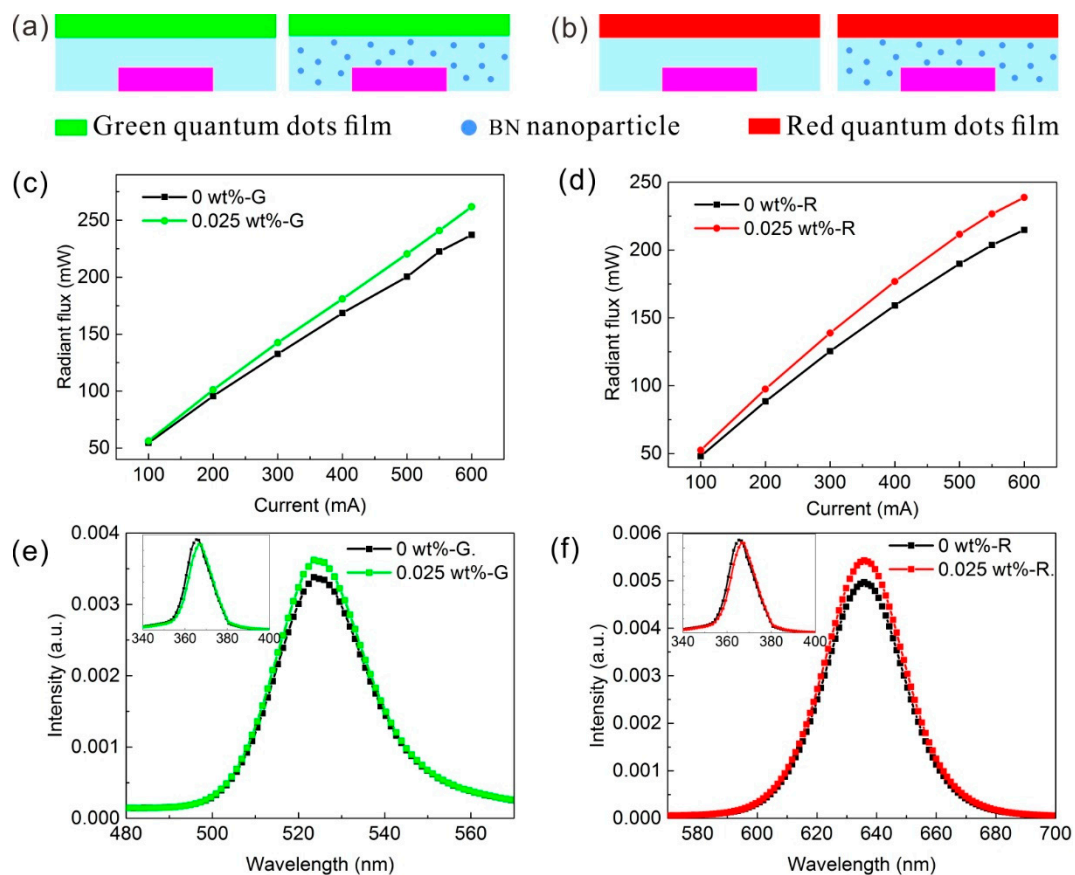


Figure 10. Schematic of UVLED excitation of (a) green quantum dot films and (b) red quantum dot films, with and without BN NPs. (c) Radiant flux of green-UVLED and (d) red-UVLED, versus current. (e) Electroluminescence spectra of green-UVLED and (f) red-UVLED, for current of 500 mA. The inset graphs (e,f) show the spread of the ultraviolet excitation peak.

For the red QD-UVLED application, the BN NPs performed a similar phenomenon. From Figure 10d, the radiant flux of the red LED with 0.025 wt% BN NPs was higher than the BN reference. Under 500 mA, the radiant fluxes of the red LED devices without and with the BN NPs were 189.9 and 211.5 mW, respectively, an increase of 11.4%. The emission spectrum showed that the red LED had both the 367 nm purple and the 636 nm red peaks. By analyzing the EL spectra of the red LEDs, the enhancement in flux from the BN-based red LED was from the increase of the red peak and the decrease of the purple. These experimental results supports that the BN NPs in the encapsulation increase the LED ultraviolet light emission. Therefore, BN NPs have potential prospects in the application of UV-sensitive quantum dots.

4. Conclusions

To investigate the suitability of various nanoparticles for UVLED application, AlN, BN, TiO₂, ZnO, and ZrO₂ NPs were compared. Sorted by reflectance from high to low, the order was BN > ZrO₂ > AlN > TiO₂ > ZnO at 365 nm, a representative UVA wavelength. BN nanoparticles, having the strongest UV reflectivity among these five kinds of nanoparticles, were selected for further study. With the introduction of BN NPs into the silicone encapsulation, the light power of the UVLED device increased and reached a peak at 0.025 wt% BN concentration before falling. The maximum improvement of the radiant flux was 8.1% compared with the non-BN NP reference, when driven at 400 mA. Film containing BN NPs was characterized; the transmittance decreased and the haze increased with increasing BN concentration. The transmission and haze were in an excellent negative linear relationship. Though a decrease in transmission would not normally be conducive to light emission, the increase in haze is

beneficial for the scattering of light, reducing the losses from total internal reflection at the air–silicone interface. The optimized light output at 0.025 wt% BN concentration shows that haze played a positive role; from 0 wt% to 0.025 wt% BN, the radiant flux was increasing, but above 0.025 wt% the decrease in transmittance dominated and the radiant flux dropped. The thermal management of the optimized UVLED was also improved due to the increased light output.

Applying this BN-based package structure to a 365 nm excited quantum dot device, the radiant flux from green and red quantum dot LED units was increased by 9.9% and 11.4% under 500 mA, respectively, by 0.025 wt% BN NPs in the UVLEDs. This improvement mainly resulted from the decrease of the ultraviolet peak and the increase of the quantum dot emission peak, indicating that more ultraviolet light was absorbed by the quantum dots in the BN-based structure. We believe this demonstrates that BN NPs have great prospects for application in UVLEDs, especially in an ultraviolet excitation source for quantum dots.

Author Contributions: Formal analysis, C.Y. and X.D.; Funding acquisition, Y.T. and Z.L.; Investigation, Q.Z. and J.L.; Methodology, Q.Z. and X.D.; Resources, J.L. and Z.L.; Writing—original draft, C.Y.; Writing—review & editing, Y.T. and Z.L.

Funding: This study was supported by the Science & Technology Program of Guangdong Province (2019B010130001); National Natural Science Foundation of China (No. 51775199, No. 51735004); Natural Science Foundation of Guangdong Province (2014A030312017); Special Funds for the Cultivation of Guangdong College Students' Scientific and Technological Innovation. ("Climbing Program" Special Funds.) (No. pdjh2018a0026).

Conflicts of Interest: The authors declare no conflict of interest.

Abbreviation

UVLED	Ultraviolet light-emitting diodes
NPs	Nanoparticles
EQE	External quantum efficiency
IQE	Internal quantum efficiency
QDs	Quantum dots
PDMS	Polydimethylsiloxane
PL	Photoluminescence
EL	Electroluminescence

References

1. Pimpulkar, S.; Speck, J.S.; Denbaars, S.P.; Nakamura, S. Prospects for LED lighting. *Nat. Photon.* **2009**, *3*, 180–182. [[CrossRef](#)]
2. Sanderson, S.W.; Simons, K.L. Light emitting diodes and the lighting revolution: The emergence of a solid-state lighting industry. *Res. Policy* **2014**, *43*, 1730–1746. [[CrossRef](#)]
3. Pust, P.; Schmidt, P.J.; Schnick, W. A revolution in lighting. *Nat. Mater.* **2015**, *14*, 454–458. [[CrossRef](#)] [[PubMed](#)]
4. Hirayama, H.; Maeda, N.; Fujikawa, S.; Toyoda, S.; Kamata, N. Recent progress and future prospects of AlGaIn-based high-efficiency deep-ultraviolet light-emitting diodes. *Jpn. J. Appl. Phys.* **2014**, *53*, 100209. [[CrossRef](#)]
5. Chen, J.; Loeb, S.; Kim, J.-H. LED revolution: fundamentals and prospects for UV disinfection applications. *Environ. Sci. Water Res. Technol.* **2017**, *3*, 188–202. [[CrossRef](#)]
6. Muramoto, Y.; Kimura, M.; Nouda, S. Development and future of ultraviolet light-emitting diodes: UV-LED will replace the UV lamp. *Semicond. Sci. Technol.* **2014**, *29*, 084004. [[CrossRef](#)]
7. Kneissl, M.; Seong, T.-Y.; Han, J.; Amano, H. The emergence and prospects of deep-ultraviolet light-emitting diode technologies. *Nat. Photon.* **2019**, *13*, 233–244. [[CrossRef](#)]
8. Würtele, M.A.; Kolbe, T.; Lipsz, M.; Külberg, A.; Weyers, M.; Kneissl, M.; Jekel, M. Application of GaN-based ultraviolet-C light emitting diodes – UV LEDs – for water disinfection. *Water Res.* **2011**, *45*, 1481–1489. [[CrossRef](#)] [[PubMed](#)]

9. Khan, A.; Balakrishnan, K.; Katona, T. Ultraviolet light-emitting diodes based on group three nitrides. *Nat. Photon.* **2008**, *2*, 77–84. [[CrossRef](#)]
10. Shur, M.S.; Gaska, R. Deep-ultraviolet light-emitting diodes. *IEEE Trans. Electron Devices* **2010**, *57*, 12–25. [[CrossRef](#)]
11. Oh, J.-T.; Moon, Y.-T.; Kang, D.-S.; Park, C.-K.; Han, J.-W.; Jung, M.-H.; Sung, Y.-J.; Jeong, H.-H.; Song, J.-O.; Seong, T.-Y. High efficiency ultraviolet GaN-based vertical light emitting diodes on 6-inch sapphire substrate using ex-situ sputtered AlN nucleation layer. *Opt. Express* **2018**, *26*, 5111–5117. [[CrossRef](#)] [[PubMed](#)]
12. Li, Z.; Cao, K.; Li, J.; Tang, Y.; Xu, L.; Ding, X.; Yu, B. Investigation of Light-Extraction Mechanisms of Multiscale Patterned Arrays With Rough Morphology for GaN-Based Thin-Film LEDs. *IEEE Access* **2019**, *7*, 73890–73898. [[CrossRef](#)]
13. Lin, H.-Y.; Sher, C.-W.; Hsieh, D.-H.; Chen, X.-Y.; Chen, H.-M.P.; Chen, T.-M.; Lau, K.-M.; Chen, C.-H.; Lin, C.-C.; Kuo, H.-C. Optical cross-talk reduction in a quantum-dot-based full-color micro-light-emitting-diode display by a lithographic-fabricated photoresist mold. *Photonics Res.* **2017**, *5*, 411–416. [[CrossRef](#)]
14. Tran, B.T.; Maeda, N.; Jo, M.; Inoue, D.; Kikitsu, T.; Hirayama, H. Performance improvement of AlN crystal quality grown on patterned Si (111) substrate for deep UV-LED applications. *Sci. Rep.* **2016**, *6*, 35681. [[CrossRef](#)] [[PubMed](#)]
15. Hu, H.; Zhou, S.; Liu, X.; Gao, Y.; Gui, C.; Liu, S. Effects of GaN/AlGaN/Sputtered AlN nucleation layers on performance of GaN-based ultraviolet light-emitting diodes. *Sci. Rep.* **2017**, *7*, 44627. [[CrossRef](#)] [[PubMed](#)]
16. Ooi, Y.K.; Zhang, J. Light extraction efficiency analysis of flip-chip ultraviolet light-emitting diodes with patterned sapphire substrate. *IEEE Photonics J.* **2018**, *10*, 1–13. [[CrossRef](#)]
17. Wang, S.; Dai, J.; Hu, J.; Zhang, S.; Xu, L.; Long, H.; Chen, J.; Wan, Q.; Kuo, H.-C.; Chen, C. Ultrahigh degree of optical polarization above 80% in AlGaIn-based deep-ultraviolet LED with moth-eye microstructure. *ACS Photonics* **2018**, *5*, 3534–3540. [[CrossRef](#)]
18. Li, Z.; Song, C.; Qiu, Z.; Li, J.; Cao, K.; Ding, X.; Tang, Y. Study on the Thermal and Optical Performance of Quantum Dot White Light-Emitting Diodes Using Metal-Based Inverted Packaging Structure. *IEEE Trans. Electron Devices* **2019**, *66*, 3020–3027. [[CrossRef](#)]
19. Schneider, M.; Leyrer, B.; Herbold, C.; Trampert, K.; Brandner, J.J. Thermal improvements for high power UV LED clusters. In Proceedings of the IEEE Electronic Components & Technology Conference, Lake Buena Vista, FL, USA, 31 May–3 June 2011.
20. Tang, Y.; Li, Z.; Li, Z.-T.; Li, J.-S.; Yu, S.-D.; Rao, L.-S. Enhancement of luminous efficiency and uniformity of CCT for quantum dot-converted LEDs by incorporating with ZnO nanoparticles. *IEEE Trans. Electron Devices* **2018**, *65*, 158–164. [[CrossRef](#)]
21. Li, J.-S.; Tang, Y.; Li, Z.-T.; Li, Z.; Ding, X.-R.; Rao, L.-S. Investigation of the emission spectral properties of carbon dots in packaged LEDs using TiO₂ nanoparticles. *IEEE J. Sel. Top. Quant.* **2017**, *23*, 1–7. [[CrossRef](#)]
22. Su, Y.-K.; Wang, P.-C.; Lin, C.-L.; Huang, G.-S.; Wei, C.-M. Enhanced Light Extraction Using Blue LED Package Consisting of TiO₂-Doped Silicone Layer and Silicone Lens. *IEEE Trans. Electron Devices Lett.* **2014**, *35*, 575–577.
23. Wang, P.-C.; Su, Y.-K.; Lin, C.-L.; Huang, G.-S. Improving Performance and Reducing Amount of Phosphor Required in Packaging of White LEDs With TiO₂-Doped Silicone. *IEEE Trans. Electron Devices Lett.* **2014**, *35*, 657–659.
24. Zheng, H.; Li, L.; Lei, X.; Yu, X.; Liu, S.; Luo, X. Optical performance enhancement for chip-on-board packaging LEDs by adding TiO₂/silicone encapsulation layer. *IEEE Trans. Electron Devices* **2014**, *35*, 1046–1048. [[CrossRef](#)]
25. Chen, J.; Hardev, V.; Hartlove, J.; Hofler, J.; Lee, E. 66.1: Distinguished Paper: A High-Efficiency Wide-Color-Gamut Solid-State Backlight System for LCDs Using Quantum Dot Enhancement Film. *SID Symp. Dig. Tec. Pap.* **2012**, *43*, 895–896. [[CrossRef](#)]
26. Tang, Y.; Lu, H.; Li, J.; Li, Z.; Du, X.; Ding, X.; Yu, B. Improvement of Optical and Thermal Properties for Quantum Dots WLEDs by Controlling Layer Location. *IEEE Access.* **2019**, *7*, 77642–77648. [[CrossRef](#)]
27. Li, J.-S.; Tang, Y.; Li, Z.-T.; Ding, X.-R.; Rao, L.-S.; Yu, B.-H. Effect of quantum dot scattering and absorption on the optical performance of white light-emitting diodes. *IEEE Trans. Electron Devices* **2018**, *65*, 2877–2884. [[CrossRef](#)]

28. Wang, X.; Li, W.; Sun, K. Stable efficient CdSe/CdS/ZnS core/multi-shell nanophosphors fabricated through a phosphine-free route for white light-emitting-diodes with high color rendering properties. *J Mater. Chem.* **2011**, *21*, 8558–8565. [[CrossRef](#)]
29. Zhang, L.; Zheng, Y.; Mao, J.; Wang, S.; Fu, R.; Yang, Y.; Yin, D.; Song, Q.; Chen, Y. Development of an Al₂O₃ filled composite for the bracket of ultraviolet light-emitting diodes (UV-LEDs). *Opt. Mater.* **2018**, *83*, 356–362. [[CrossRef](#)]
30. Bae, J.-Y.; Kim, Y.; Kim, H.; Kim, Y.; Jin, J.; Bae, B.-S. Ultraviolet light stable and transparent sol-gel methyl siloxane hybrid material for UV light-emitting diode (UV LED) encapsulant. *ACS Appl. Mater. Interfaces* **2015**, *7*, 1035–1039. [[CrossRef](#)]
31. Kim, K.I.; Choi, S.C.; Kim, J.H.; Cho, W.S.; Hwang, K.T.; Han, K.S. Synthesis and characterization of high-purity aluminum nitride nanopowder by RF induction thermal plasma. *Ceram. Int.* **2014**, *40*, 8117–8123. [[CrossRef](#)]
32. Lee, K.H.; Jeong, S.M.; Kwon, W.T.; Kim, S.R.; Shin, D.G.; Kim, H.S.; Kim, Y. Purification and Size Control of AlN Powder for AlN Single Crystal Growth. *Mater. Sci.* **2014**, *804*, 107–110. [[CrossRef](#)]
33. Golberg, D.; Bando, Y.; Huang, Y.; Terao, T.; Mitome, M.; Tang, C.; Zhi, C. Boron nitride nanotubes and nanosheets. *ACS Nano* **2010**, *4*, 2979–2993. [[CrossRef](#)] [[PubMed](#)]
34. Ding, X.; Yong, T.; Li, Z.; Qiu, C.; Li, Y.; He, Y. Thermal and optical investigations of high power LEDs with metal embedded printed circuit boards. *Int. Commun. Heat Mass Transfer.* **2015**, *66*, 32–39. [[CrossRef](#)]
35. Ding, X.; Li, M.; Li, Z.; Tang, Y.; Xie, Y.; Tang, X.; Fu, T. Thermal and optical Investigations of a laser-driven phosphor converter coated on a heat pipe. *Appl. Therm. Eng.* **2019**, *148*, 1099–1106. [[CrossRef](#)]
36. Chen, H.C.; Chen, K.J.; Wang, C.H.; Lin, C.C.; Yeh, C.C.; Tsai, H.H.; Shih, M.H.; Kuo, H.C.; Lu, T.C. A novel randomly textured phosphor structure for highly efficient white light-emitting diodes. *Nanoscale Res. Lett.* **2012**, *7*, 188. [[CrossRef](#)]



© 2019 by the authors. Licensee MDPI, Basel, Switzerland. This article is an open access article distributed under the terms and conditions of the Creative Commons Attribution (CC BY) license (<http://creativecommons.org/licenses/by/4.0/>).